Biosensors and Bioelectronics 124–125 (2019) 176–183

Contents lists available at ScienceDirect

Biosensors and Bioelectronics

journal homepage: www.elsevier.com/locate/bios

Enantioselective analysis of D- and L- Serine on a layer-by-layer imprinted electrochemical sensor

Swadha Jaiswal, Richa Singh, Kislay Singh, Sana Fatma, Bhim Bali Prasad*

Analytical Division, Department of Chemistry, Institute of Science, Banaras Hindu University, Varanasi 221005, India

ARTICLE INFO

Keywords:
Dual imprinted polymer
Layer-by-Layer
Graphene
Fullerene
D- and L-Serine
One-by-one approach

ABSTRACT

The present work describes a new, simple, and easy method of generating acrylamide functionalised reduced graphene oxide-fullerene layer-by-layer assembled dual imprinted polymers to quantify D- and L-Serine at ultra trace level in aqueous and real samples. Herein, the pencil graphite electrode was initially spin coated with D-Serine imprinted acrylamide functionalized reduced graphene oxide. After 10 min thermal treatment (50 °C), this electrode was again modified with L-Serine imprinted acrylamide functionalized fullerene molecules. This bilayer assembly was finally made thermally stable by 60 °C exposure for 3 h. The proposed sensor showed better electronic properties with an improved synergism. We have compared this modified electrode with other modified pencil graphite electrodes like single layered acrylamide functionalised reduced graphene oxide or fullerene, single layered acrylamide functionalised reduced graphene oxide-fullerene composite and double layered acrylamide functionalised reduced graphene oxide or fullerene molecules, which yielded very inferior sensitivity due to possible agglomeration and decreased synergism. The chosen system demonstrated a very good analytical figures of merit with differential pulse anodic stripping voltammetry and cyclic voltammetry transduction, showing lower limits of detection (0.24 ng mL^{-1}, $S/N = 3$) for both isomers. The proposed sensor assures practical applications as disease biomarker, manifesting several diseases at very ultra-trace level.

1. Introduction

Analysis of biomarkers is a fascinating field in sensor development (Bozkurt et al., 2017; Başkaya et al., 2017; Hu et al., 2018; Koskun et al., 2018; Saraf et al., 2018). The deficiency and excess of biomarkers in body are the major causes behind all diseases. This warrants an increased demand to devise a fool-proof technology for better detection. Implementation of electrochemical devices could be considered effective for rapid, specific, and inexpensive mean of biomarker analysis (Labib et al., 2016)

In the present work, an electrochemical sensing platform is integrated with molecularly imprinting technology to detect D- & L- Serine (D-Ser and L-Ser) in real samples utilizing a layer-by-layer (LbL) approach. LbL assembly is a rich, versatile, and powerful technique for fabricating multilayer thin film with controlled architecture and functions (Xu et al., 2012). Simply put, molecularly imprinted polymer (MIP) is a system inherited with the memory of the shape, size, and the functional groups of a target molecule. MIP is designed by imprinting test analyte in polymer motif and creating void spaces through retrieval of template, which later on found very elegant for specific recognition of template analyte in the real world samples (Vasapollo et al., 2011). It has been found that if two isomers are templated in two different MIP layers, separated by acrylic moiety, the isomers selectivity is better, showing absolutely no criss-cross diffusion, in comparison with the single layer imprinted MIP motif or double layer imprinted MIPs of identical structure (Prasad et al., 2017a, 2017b). Thus, the two MIP layers ought to be made of two different motifs for better selectivity of two isomers.

If the hybrid heterostructure are in same plane of modification, the electrical and mechanical properties of the film may be hampered due to some sort of agglomeration of hybrid structure (Kouloumpis et al., 2015). Therefore, we have taken privilege to employ two different allotropes of carbon, like graphene oxide and fullerene (C_{60}), in LbL synthesis. This facilitates to formulate a good conducting LbL polymer with inherent properties like large surface area, better electrical conductivity, and rich edge sites. Graphene oxide and fullerene have itself possess unique electronic properties with strikingly strange chemistry which together gets several times enhanced properties in various perspectives (Spyrou et al., 2013; Georgakilas et al., 2016a, 2016b; Bourlinos et al., 2017; Chernozatonskii et al., 2016). It has already been discovered that graphene coverage with C_{60} molecules improves significant electron transport, since C_{60} (0D) is acceptor of electrons and

* Corresponding author.
E-mail address: prasadbb_2015@yahoo.com (B.B. Prasad).

https://doi.org/10.1016/j.bios.2018.09.090
Received 23 July 2018; Received in revised form 21 September 2018; Accepted 27 September 2018
Available online 28 September 2018
0956-5663/

graphene (2D) is a well known electron donor (Dickert et al., 2001). More explicitly, the addended C_{60}-molecules and reduced graphene oxide (rGO) sheets possess much appealing uses in sensing field, by enhancing electrochemical properties of films by decreasing their resistivities. Presence of enormous π-orbitals in rGO permits higher heterogeneous electron transfer rates (Martín and Escarpa, 2014). We have thus formulated highly conducting polymeric films comprising acrylamide functionalized rGO and acrylamide functionalized C_{60} molecules. The acrylamide functions of both carbon allotropes were essentially required to generate vinylic bonds for consumption in the surface polymerization and formation of hybrid heterostructure via LbL process. The polymerization was feasible by activator generated atom transfer radical polymerization technique (ARGET-ATRP) (Tang et al., 2006). The two MIP layers, imprinted with D- & L- Serine, respectively, are stalked one over the other via vinylic bonds including π-π interactions. Combination of two different target molecules (enantiomers) in two MIP layers enabled the creation of hollows for analyte re-inclusion via hydrogen bondings, with improved diffusion pathways, time saving and cost-effective (Jing et al., 2010).

Serine, a non-essential amino acid, plays central role in cellular proliferation and is essential for the functioning of central nervous system (Wu, 2009). L-Ser contributes to functioning of RNA and DNA, muscles formation, fat/fatty acids metabolism, and maintenance of immune system (Koning et al., 2003). D-Ser, an endogenous amino acid, possesses unique neurotransmitter characteristics. D-Ser acts as obligatory coagonist at the glycine site associated with the N-methyl-D-aspartate subtype of glutamate receptors (NMDAR) and has a cardinal modulatory role in neurotransmission, neurotoxicity, synaptic plasticity, and cell migration (Singh and Singh, 2016). It is thus essential to monitor D-Ser and L-Ser together for clinical therapy of patients suffering psychiatric disorders. D & L- Ser levels in serum is 1.89 ng mL^{-1} and 159.74 ng mL^{-1}. It is, however, lowered to 1.47 ng mL^{-1} for D- Ser and raised to 167.09 ng mL^{-1} for L-Ser, respectively in a schizophrenic patient (Hashimoto et al., 2003). Normal D-Ser and L-Ser cerebrospinal fluid (CSF) levels are 189.16 ng mL^{-1} and 1909.54 ng mL^{-1} and increased to 533.59 ng mL^{-1} and 1694.09 ng mL^{-1}, respectively in a hydrocephalus patient (Madeira et al., 2015).

Various electroanalytical methods are reported for serine estimation namely, imprinted polycrystalline nickel-nickel oxide half nanotube-modified boron-doped diamond electrode (Dai et al., 2015), amperometric determination on NiO nanoparticle-modified glassy carbon electrode (Roushani et al., 2012), and voltammetric determination using bamboo charcoal derived carbon nanosphere electrode (Saha and Das, 2014). Other reported methods involve piezoelectric estimation using imprinted copolymer casted on gold surface of quartz crystal (Jegal et al., 2007), imprinted sol-gel (Fernandez-Gonzalez et al., 2011), chiral separation of D- and L-Serine racemate by a MIP membrane (Son and Jegal, 2007), MIP sensor for serine on carbon nanotube (Halim et al., 2013), and sensor based on graphene sheet Congo-red MIP and organic thin film transistor (Halim et al., 2014). So far reported techniques possess various shortcomings like cross interferences, labour intrusive, time consuming, etc. These are, however, much more surmounted through the present work.

It may be borne in mind that this work is being reported for the first time as no work is, hitherto, reported in the literature for D- and L-serine analysis present as mixture in real samples. Since both forms of D- and L-Ser give overlapped electrochemical peaks, it was imperative to apply one-by-one approach (Prasad et al., 2017a, 2017b) for enantioselective analysis. Accordingly, one has to saturate the imprinted cavities of D-Ser while quantifying L-Ser, and vice-versa. Double imprinting is seldom made due to its underlying apprehension of limited success in molecular recognition owing to criss-cross diffusion of analytes. The situation is more worsened if chiral compounds are analysed which gives overlapped voltammetric peaks due to their identical redox behaviour. Although MIP-sensors are known for individual analysis of optical isomers using two separate electrodes (Prasad et al., 2013, 2014), the proposed method is novel utilizing the sequential approach of analyzing two enantioselective isomers at one electrode surface duly modified with Lbl dual imprinted polymers of acrylamide functionalized rGO and C_{60}. The preparative protocols of the proposed sensor are relatively very easy and repetitive. The modified PGE sensor so produced is more sensitive, accurate and time-saver avoiding any cross-reactivity and diffusional constraint.

2. Experimental

2.1. Chemicals and reagents

Analytical grade reagents are utilized without further purification. Demineralized triple distilled water (conducting range 0.06–0.07 × 10^{-6} S cm^{-1}) was used in all experiments. Tert-butyl bromoacetate, dimethyl sulphide, p-toulene sulfonic acid, carbon disulphide, hydrazine, acrylamide, D-Ser, and L-Ser were acquired from Sigma-Aldrich (Steinheim, Germany). Potassium ferricyanide, thionyl chloride ($SOCl_2$) and $KMnO_4$ were purchased from Loba chemie (Mumbai, India). Copper chloride ($CuCl_2$), graphite powder, bipyridyl, acetic acid, sodium hydroxide (NaOH), nitric acid (HNO_3), sulphuric acid (H_2SO_4), and all interferents were purchased from Fluka (Steinheim, Germany). All solvents, dimethyl sulphoxide (DMSO), tetrahydrofuran (THF), triethylamine (TEA), dimethyl formamide (DMF), dioxane, carbon disulphide (CS_2), toluene, acetone, chloroform, methanol, and ethanol were procured from Spectrochem Pvt. Ltd. (Mumbai, India). C_{60} (> 99.0%) was procured from the Tokyo Chemicals Industries Co. Ltd. (Tokyo, Japan). The supporting electrolyte used was phosphate buffer solution (pH 13, ionic strength 0.01 M). Standard stock solutions of D-Ser and L-Ser (500 μg mL^{-1}) and potassium ferricyanide (30 ng mL^{-1}) were prepared in water. All working solutions were prepared by diluting stock solution with water. Commercially available amino acid tablets were purchased from Universal Medicare Pvt. Ltd. (Mumbai, India). Human blood serum and CSF were obtained from the Institute of Medical Science, Banaras Hindu University (Varanasi, India) and kept in refrigerator below 4 °C, before use. Pencil rods (2B grade, 2 mm diameter, 5.0 cm length) were purchased from Hi Par, Camlin Ltd. (Mumbai, India). The details of instruments used in this work are provided in the Supporting Information Section S.1.

2.2. Synthesis of graphene oxide (GO)

Hummer's method was utilized for the preparation of graphene oxide (GO) from graphite powder (Hummers and Offeman, 1958). In short, graphite powder (0.5 g) was oxidized in HNO_3 (10.0 mL) and H_2SO_4 (1:3, v/v) mixture and refluxed for 48 h. The pre-oxidized graphite was centrifuged, washed with dry THF and vacuum dried. The obtained material was oxidized with mixture of 96% H_2SO_4 (20 mL) and $KMnO_4$ (2.0 g) by refluxing (3 h). At last GO was collected and vacuum dried.

2.3. Reduction to rGO and its acylation

GO (0.1 g) dispersed in DMF was reduced by refluxing it with hydrazine (2.0 mL) for 24 h. The resultant rGO was centrifuged, washed with dry THF and vacuum dried. This product (0.06 g) in DMF (2.0 mL) was sonicated for 45 min and treated with $SOCl_2$ (6.0 mL) at 80 °C for 48 h. The acyl group functionalized rGO (rGO-COCl) so obtained was centrifuged, washed with anhydrous THF, and vacuum dried.

2.4. Preparation of C_{60}-COCl (Acylation of fullerene)

For the synthesis of C_{60}-COCl, the starting reagent, *tert*-Butyl (dimethylsulfanylidene) acetate, was prepared from *tert*-butyl bromoacetate according to the method reported earlier (Tada et al., 2006). The

prepared *tert*-Butyl (dimethylsulfanylidene) acetate (0.004 g, 0.5 mL toluene) was added into C_{60} solution (0.020 g, 20.0 mL toluene), stirred at room temperature for 18 h, and concentrated under reduced pressure. The resultant residue was collected to afford *tert*-butyl C_{60}-acetate as a brown solid. A toluene solution (10.0 mL) of *tert*-Butyl C_{60}-acetate (0.010 g) and *p*-toluene sulfonic acid (0.004 g) was refluxed for 8 h to generate a suspension. The brown solid thus precipitated was collected by filtration and washed successively with toluene: water (3:1 v/v). The residual solid was dissolved in CH_2Cl_2/dioxane (1:1 (v/v), 5 mL) and the insoluble mass was filtered off. The filtrate was concentrated to dryness to afford C_{60}-acetic acid as a brown solid. A solution of C_{60}-acetic acid (0.008 g) and $SOCl_2$ (1.0 mL) in CH_2Cl_2/ dioxane (1:1 v/v, 5.0 mL) was refluxed for 5 h to afford a black precipitate. The precipitate was collected by filtration and washed with CH_2Cl_2/dioxane (1:1 v/v, 10.0 mL). The residual solid was dissolved in CS_2 (5.0 mL), and the insoluble mass was filtered off. The filtrate was concentrated to dryness to give C_{60}-COCl as a black solid (Tada et al., 2006).

2.5. Vinyl group modification of acylated rGO and C_{60}

The freshly prepared rGO-COCl (0.10 g) and C_{60}-COCl (0.10 g) are separately treated with acrylamide (0.20 g) followed by dilution with 5.0 mL water. These mixtures were sonicated for 1 h. The so produced products were refluxed with $SOCl_2$ (2 mL) at 80 °C for 72 h. The final products (acrylamide functionalised rGO and acrylamide functionalised C_{60}) were subjected to centrifugation, washed with anhydrous THF, and finally dried in vacuum (Xu et al., 2014).

2.6. Synthesis protocol for layer-by-layer assembled imprinted polymers on the surface of pencil graphite electrode (PGE)

LbL assembly of imprinted polymeric films were grafted on the surface of PGE. The fabrication involved following steps. Firstly, a pre-polymer mixture was made in DMSO constituting acrylamide functionalised rGO (0.1 g, 1.0 mL DMSO), template (D-Ser, 0.05 g, 1.0 mL DMSO), catalyst [Cu-II complex obtained by mixing $CuCl_2$ (0.01 mmol) and bpy (0.01 mmol) in 1.0 mL DMSO], reducing agent (TEA, 200.0 μL), and initiator (chloroform, 100.0 μL). The pre-polymerization mixture was purged with N_2 (10 min). This solution (15.0 μL) was spin coated (2500 rpm, 30 s) at the surface of PGE and subjected to 50 °C for 10 min to stabilize the layer. Secondly, for next layer architecture, a pre-polymer mixture of acrylamide functionalised C_{60} (0.1 g, 1.0 mL DMSO), template (L-Ser, 0.05 g 1.0 mL DMSO), catalyst [Cu-II complex obtained by mixing $CuCl_2$ (0.01 mmol) and bpy (0.01 mmol) in 1.0 mL DMSO], reducing agent (TEA, 200.0 μL), and initiator (chloroform, 100.0 μL) was purged with N_2 gas for 10 min. This solution (15.0 μL) was spun on the first layer of acrylamide functionalised rGO at 2500 rpm for 30 s at the surface of PGE and air dried. After the LbL deposition of polymer films, the electrode was thermally treated for an additional 3 h at 60 °C to ensure complete polymerization, as depicted in Scheme 1. Both template molecules were removed from their respective MIP-adducts by plunging the modified electrode into acetic acid–methanol (1:8, v/v) mixture for 30 min. The complete template(s) extraction was evinced until no voltammetric response of the template (s) was found. A double layer of non-imprinted polymer (NIP) modified electrode was also fabricated as mentioned above, but in the absence of template(s).

2.7. Electroanalytical measurements

The electrochemical behaviour of acrylamide functionalised rGO-C_{60}/MIP (LbL)/PGE in 10.0 mL of 0.01 M phosphate buffer (pH 13) was investigated. After the blank run, the L-Ser was added to the cell for accumulation at 0.3 V vs Ag/AgCl for 120 s followed by 15 s equilibration time. This yielded DPASV runs for L-Ser in the potential range varying from − 0.4–0.6 V (vs Ag/AgCl) at a scan rate 10 mV s^{-1}, pulse amplitude 25 mV, and pulse width 50 ms, till saturation until a constant DPASV current (I') was attained, without any further increase of L-Ser. At this stage, cavities specific to D-Ser were set free to recapture D-Ser and give DPASV currents (I). Thus, the oxidation current ($\Delta I = I - I'$) versus D-Ser concentration profile was obtained. The modified electrode was regenerated by retrieving both templates for the next use for L-Ser estimation following the similar steps as stated in the D-Ser estimation. Accordingly, molecular cavities for D-Ser were saturated and L-Ser was evaluated on the same electrode. CV experiments were performed within the same potential window as DPASV in anodic stripping mode.

Since dissolved oxygen present in the cell did not affect the current response, any deaeration of the cell content was not necessary. This was evinced by taking DPASV/CV runs in the presence and absence of N_2 purging, which responded similar results. The limit of detection (*LOD*) was calculated as three times the standard deviation for the blank measurement in the absence of target analyte divided by the slope of the calibration plot.

3. Results and discussion

3.1. About polymeric films

Conducting properties of polymeric films developed in this work were compared. For this, DPASV signals of $K_3[Fe(CN)_6]$ probe molecules (0.01 mM) in phosphate buffer (pH 13) were obtained (Fig. 1). Accordingly, of all duly modified working electrodes such as acrylamide functionalised rGO/MIP (single layer), acrylamide functionalised C_{60}/MIP (single layer), acrylamide functionalised rGO-C_{60}/MIP (single layer), acrylamide functionalised rGO /MIP(LbL), and acrylamide functionalised C_{60}/MIP (LbL), the acrylamide functionalised rGO-C_{60}/MIP(LbL) has been found to demonstrate a highest current. Thus, we have selected acrylamide functionalised rGO-C_{60} imprinted PGE for this work. It is reported that LbL polymers prepared from two monomers show better binding capacity and recognition abilities compared to polymers prepared by single monomer (Antwi-Boampong et al., 2014). Furthermore, it is advantageous to take bilayer architecture as it increases adsorption kinetics (Venkatesan et al., 2015). We have utilized r-GO as the bottom layer since it effectively enhances the transduction mechanism by making the sensor more selective (Hernández et al., 2012).

By switching the design of film from single layer to LbL, a 2-fold enhancement in DPASV signals was noticed (Fig. 1). Herein, acrylamide functionalised rGO acts as a high performance support while acrylamide functionalised C_{60} showed an uniformly adherence as top layer. In fact, this particular design showed the synergistic effect to induce enormous porosity favouring conductivity. In this fashion, the two layers actually held together via vinylic bond to stabilize the structure with elegance electronic properties. Herein, the uses of hybrid graphene-based thin multi-layers have advantages of the precise control and the homogenous deposition over large area, through vinylic bonds, making the LbL technique promising for preventing agglomeration, with modified tuned and enhanced electronic and mechanical properties (Kouloumpis et al., 2015). Furthermore, the hybrid material can generate some synergistic and exciting performance than the individual materials (Zaidi and Shin, 2014). Although several heterostructures based on graphene-fullerene (Ma et al., 2013), graphene molybdenum disulphide monolayer decorated C_{60} (Chang et al., 2014), and graphene carbon nanotubes (Yáñez-Sedeño et al., 2010; Singh et al., 2011) have been reported in same layer of modification exploiting weak vanderwaal physisorptions, these have reportedly some sort of agglomeration between carbon-based nanostructure during the film synthesis (Kouloumpis et al., 2015). This may cause somewhat inferior synergistic performance than acrylamide sandwiched hybrid heterostructure of graphene-C_{60}, in two distinct layers of LbL films. It appears

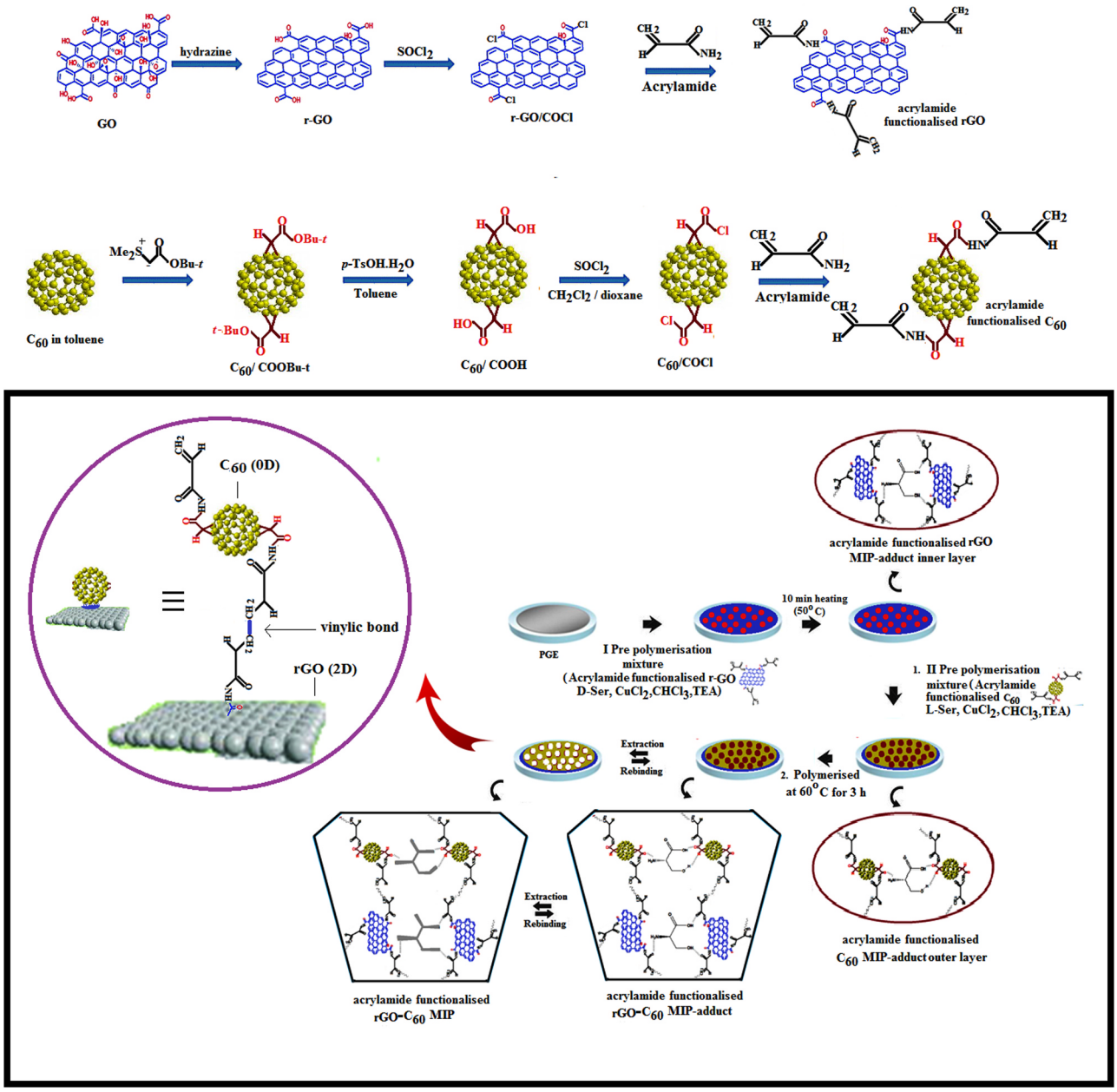

Scheme 1. Schematic development of acrylamide functionalised rGO-C_{60}/MIP (LbL)/PGE.

that C_{60} (0D) and graphene oxide (2D), sandwiched by acrylamide functionalities, have lower agglomeration and a higher degree of synergism because of two layers deposited in two different planes (Scheme 1, inserted as circle). Furthermore, the non-covalent hydrogen bondings between the LbL film and templates(s) may induce a high degree of dispersability, bio-compatibility, reactivity, binding capacity, and sensing properties (Georgakilas et al., 2016a, 2016b). Virtually, the 'pore geometry' of C_{60} subdued the negative aspect of increased thickness of bilayer film by granting an easier diffusional pathway to analyte(s) and channelize electron transportation through r-GO to the electrode surface (Bozdaganyan et al., 2014).

For developing imprinted network, different template-monomer weight ratios (1:1, 1:2, 1:3, 1:4) were attempted to explore an optimum stoichiometry between the MIP and template (s) complex.. [For details on template extraction, stoichiometry of MIP-adduct(s) and optimization of polymerization conditions, vide Supporting Data Section S.2. and Fig. S1]

3.2. Electrochemistry

Electrochemistry of bare PGE, acrylamide functionalised rGO-C_{60} MIP (single layer), and acrylamide functionalised rGO-C_{60}/ MIP (LbL) modified PGEs were studied with the help of $[Fe(CN)_6]^{3-/4-}$ redox probe in phosphate buffer (pH = 13) (Fig. 2). The current gradually increased from bare to acrylamide functionalised rGO-C_{60}/MIP(single layer) and further to acrylamide functionalised rGO-C_{60}/MIP (LbL)/PGEs. The peak separation (ΔE_p) on the bare PGE, acrylamide functionalised rGO-C_{60}/MIP (single layer), and acrylamide functionalised rGO-C_{60}/MIP (LbL) modified PGEs are found to be 174, 105, and 78 mV, respectively. This indicated that not only the conductivity but the tendency for reversibility was also improved upon modification of PGE, when acrylamide functionalised rGO-C_{60}/MIP (LbL) was used for modification. Further details on electron transfer kinetics were studied in the Supporting Information Section S.3.

Electron transfer properties were further characterized by EIS.

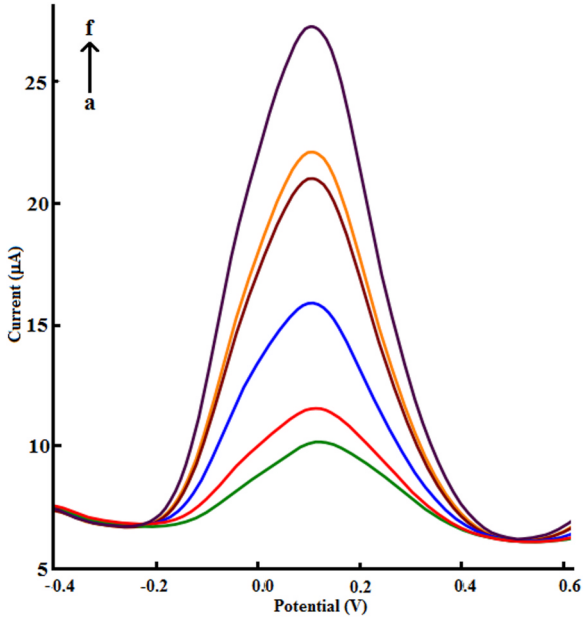

Fig. 1. DPASV response of 0.01 mM $[Fe(CN)_6]^{3-}$ on PGEs modified with (a) acrylamide functionalised r-GO/MIP (single layer), (b) acrylamide functionalised C_{60}/MIP (single layer), (c) acrylamide functionalised r-GO-C_{60}/MIP (single layer), (d) acrylamide functionalised r-GO/ MIP (LbL), (e) acrylamide functionalised C_{60}/MIP (LbL), and (f) acrylamide functionalised r-GO-C_{60}/MIP (LbL).

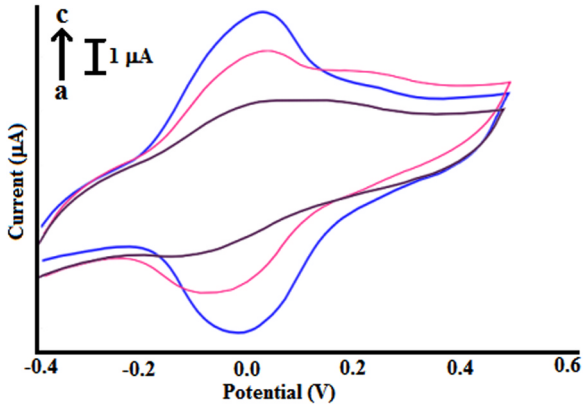

Fig. 2. Cyclic voltammograms at scan rate 100 mV s^{-1}: (a) bare PGE, (b) acrylamide functionalised r-GO-C_{60}/MIP (single layer), and (c) acrylamide functionalised r-GO-C_{60}/MIP (LbL) modified PGEs [phosphate buffer solution (pH = 13.0) containing 0.01 mM $Fe(CN)_6]^{3-/4-}$].

Accordingly, the charge transfer resistance (R_{CT}),that is determined by the diameter of the semicircle in the Nyquist plot (Fig. S2), showed relatively low charge (electron) transfer resistance (Fig. S2) The involved heterogeneous electron transfer rate constant (k_{et} = 2.36 × 10^{-3} cm s^{-1}) for $[Fe(CN)_6]^{3-/4-}$ redox couple on acrylamide functionalised rGO-C_{60}/MIP (LbL)/PGE was found to be higher than those realized with other electrodes (For details on R_{ct} and K_{et} values, vide Supporting information Section S.4). Furthermore, the heterogenous electron transfer represented by peak-to-peak separation (ΔE_p = 78 mV) indicated faster electron transfer for the present sensor, despite its larger Rct value = 350.2 Ω, as compared to an earlier work (ΔE_p = 207 mV), Rct value = 163.7 Ω (Bourlinos et al., 2017). This may be attributed to the synergistic effect on account of Lbl coatings on the electrode, despite it registered some resistance to the redox probe transportation at the bilayer junction of insulating acrylated moeties. Nevertheless, the proposed combination of acrylamide functionalised rGO and acrylamide functionalised fullerene on PGE showed better overall performance, i.e., lower potential of detection and better reversibility of the system compared to other biosensors based on reduced graphene oxide/ carbon dots composites (Hu et al., 2014), $PMo_{11}V$@ Ndoped few layer graphene (Fernandes et al., 2015) or fullerene-hollow microsphere modified gold electrodes (Wei et al., 2012).

All operating conditions of electrochemical analysis were optimized in aqueous conditions with acrylamide functionalised rGO-C_{60}/MIP (LbL)/PGE. Accordingly, the accumulation potential (E_{acc}), the accumulation time (t_{acc}), and pH of the phosphate buffer, were obtained as 0.3 V (versus saturated Ag/AgCl), 120 s, and 13, respectively, for maximum growth of DPASV signal (Fig. S3). Simultaneous analysis of D-Ser and L-Ser is problematic owing to their overlapped oxidation peaks. The mechanism for the detection of D- and L-Ser with the help of the current sensor is discussed in the Supporting Information Section S.5. In the present work, on account of the overlapping redox behaviour of D- and L- Ser, one-by-one evaluation of D-Ser and L-Ser was adopted. For this, L-specific cavities were presaturated with L-Ser molecules (20.82 ng mL^{-1}) till no increase of DPASV current occurred. It was then subjected to the D-Ser measurement by exposing D-Ser solution of different concentrations containing phosphate buffer (pH 13), for 120 s accumulation (Fig. 3A). At this stage, both D-specific and L-specific cavities were completely saturated, which was refreshed by retrieving both templates. Similar to above, D-Ser specific cavities were blocked by saturating with D-Ser molecules (20.65 ng mL^{-1}) and L-specific cavities were utilized for L-Ser estimation (Fig. 3B).

The CV runs in anodic stripping mode explored results in similar fashion as described above (Fig. S4A-B). CV investigation in aqueous solution of D-Ser (or L-Ser) (15.24 ng mL^{-1}) indicated that the oxidation peak potential (E_{pa}) of D-Ser (or L-Ser) was shifted anodically with scan rates (10–200 mV s^{-1}) (Fig. S5). Accordingly, E_{pa} vs log ν and I_{pa} *vs* $\nu^{1/2}$ profiles were represented as:

$$E_{pa}(V) = (0.050 \pm 0.001)\, log\ \nu + (0.300 \pm 0.001)(R^2 = 0.990) \quad (1)$$

$$I_{pa}(\mu A) = (15.801 \pm 2.516)\, \nu^{1/2} + (0.925 \pm 2.145)(R^2 = 0.978) \quad (2)$$

As analyte peak current (I_{pa}) increased linearly with the increase of scan rate (ν), the analyte stripping in the present instance was basically termed to be a diffusion process. Furthermore, the anodic peak potential shifted more positively while cathodic peak potential shifted more negatively, with pH (3.0–13.0). This signifies larger peak separation, in accordance to the following linear equation, with involvement of one proton in electon transportation;

$$E_{pa}(V) = (0.055 \pm 0.001)pH + (0.408 \pm 0.001)(R^2 = 0.99) \quad (3)$$

In this work, DPASV was preferred to CV for the quantitative analysis because of its relatively high sensitivity in sufficient time scale of voltammetric measurement. Accordingly, the DPASV current measured could be related to the concentration (C) of analyte in accordance with the regression equations potrayed in Table 1. The current increased had attained a constancy above 20.80 ng mL^{-1} for both the isomers, due to binding sites saturation. The non-imprinted modified electrode revealed insignificant current response upon analyte spiking (Fig. 3), which indicated an excellent imprinting phenomenon.

3.3. Spectral and surface characterizations

The provisory interactions between monomer and template were visualized by FT-IR (KBr) spectra (Fig. S6). Accordingly, the monomer (acrylamide functionalised r-GO and acrylamide functionalised C_{60}), template (Ser), MIP-adduct(s), and MIP (template-free), were comparatively studied. The FT-IR study confirms the complexation between the monomer and template(s) via hydrogen bondings which was indicated by the downward shifts of their respective key bands participating in the adduct formation. [For details on IR characteristics, vide Supporting Data Section S.6 and Fig S6]. Raman spectra of rGO and C_{60}

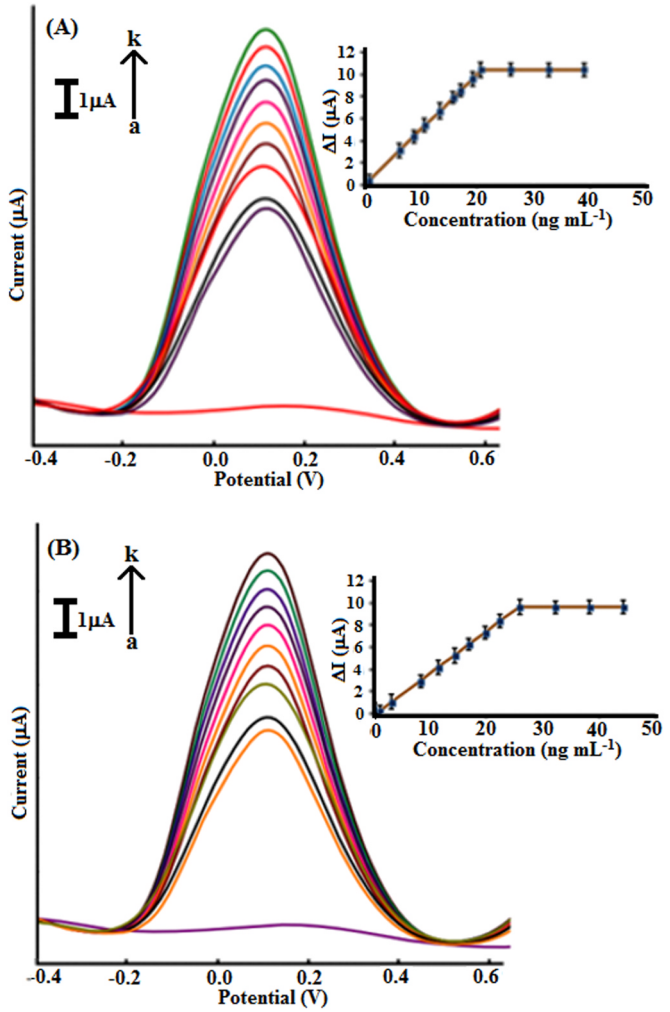

Fig. 3. (A) DPASV response of D-Ser on acrylamide functionalised r-GO-C_{60}/MIP(LbL)/PGE in aqueous solution with L-Ser saturated (20.82 ng mL^{-1}) cavities: (c-k) spiking with different D-Ser concentrations 0.83, 6.19, 8.72, 10.64, 13.38, 15.72, 16.99, 19.18, 20.63 ng mL^{-1}; curve 'b' represents DPASV response at saturation point with L-Ser cavities; and curve 'a' represents DPASV current on acrylamide functionalised r-GO-C_{60}/NIP(LbL)/PGE [operating conditions: E_{acc} 0.3 V, t_{acc} 120 s, pH 13.0, and scan rate 10 mV s^{-1}]. B) (A) DPASV response of L-Ser on acrylamide functionalised r-GO-C_{60}/MIP (LbL)/PGE in aqueous solution with D-Ser saturated (20.65 ng mL^{-1}) cavities: (c-k) spiking with different L-Ser concentrations 0.87, 2.53, 6.63, 9.09, 11.42, 13.38, 15.72, 17.78, 20.56 ng mL^{-1}; curve 'b' represents DPASV response at saturation point with D-Ser cavities; and curve 'a' represents DPASV current on acrylamide functionalised r-GO-C_{60}/NIP(LbL)/PGE. [operating conditions same as Fig. 3(A)].

along with their functionalisation are discussed in the Supporting Data Section S.7, which supported the modification of the structure.

SEM images of MIPs-adduct did not clearly showed any rGO as it is in bottom layer. However, one may visualize acrylamide functionalised rGO MIP-adduct (D-Ser) initially coated on the surface of PGE (Fig. 4A) as having sheet-like morphology with characteristically crumpled and rough architecture. As this modified electrode was again coated with acrylamide functionalised C_{60} MIP adduct (L-Ser), it showed spherically compact polymer network (Fig. 4B). On template removal, the distinct pores of different depths and apertures with spherical fullerene over rGO sheets were obtained (Fig. 4C). Fig. 4D displays the side view of acrylamide functionalised rGO-C_{60} MIP with clear boundary of rGO sheet and spherical C_{60} double layered structure and film thickness was noticed to be 130 nm. Surface morphologies were further supported from AFM images, recorded under semi-contact mode, for acrylamide functionalised rGO-C_{60}/MIP (LbL) adduct (Fig. S7A) and acrylamide functionalised rGO-C_{60}/MIP (LbL) (Fig. S7B). This provided film thickness of 131 nm – a value very close to that obtained with SEM data [For details on AFM morphology, vide Supporting Data Section S.8.]

3.4. Enantioselectivity and cross-selectivity

Imprinted layers for their enantioselectivity and cross reactivity with respect to functionally and structurally similar interfering agents, viz., aspartic acid (Asp), tryptophan (Trp), proline (Pro), uric acid (Uri), Dopamine (Dopa), Alanine (Ala), tyrosine (Tyr), cysteine (Cys), glycine (Gly), asparagine (Asn), glutamine (Gln), phenylalanine (Phe), histidine (His), and methionine (Met), were investigated. The proposed sensor was slightly responsive (Fig. S10), prior to water washing treatment, for some of the interferents. These responses could be termed as non-specific and false-positives. In fact, such non-specific contributions were first noticed on the corresponding acrylamide functionalised rGO-C_{60}/NIP (LbL)/PGE for some of interferents (Fig. S10). Such contributions were easily be vanished by water washings (n = 2, 0.5 mL) (Fig. S10). Therefore, the working electrode should be given similar washings to protect any false-positive. In a parallel work with binary mixtures of the template(s) and interferent(s), concomitantly present in 1:10 concentration ratio, the acrylamide functionalised rGO-C_{60}/MIP (LbL)PGE showed only response for the template(s) in question (Fig. S10). Virtually no cross reactivity like template-template and template-interferent(s) was observed. In other words, D-specific acrylamide functionalised rGO-C_{60}/MIP (LbL) PGE could not respond L-Ser and vice-versa and stereochemical selectivity is fully preserved in the presence of template(s). Any molecule that is smaller (Gly, Pro, Ala), larger (Uri, dopa, Asn, Glu, His, Phe, Trp, Met, Tyr) and similar (Cys, Asp) in size than D-and L-Ser could not be detected on the proposed sensor. Imprinting factors ($\alpha = \Delta i_{\text{MIP@PGE}} / \Delta i_{\text{NIP@PGE}}$) for both the templates (D- and L-Ser) were found as high as 25.68 and 25.19, respectively, using acrylamide functionalised rGO-C_{60}/ MIP (LbL)/PGE, when no washing treatment was given (Tables S2 and S3). The selectivity coefficient (k) and the relative selectivity coefficient (k') of both the enantiomers with respect to interferents were also calculated (Tables S2 and S3). The results for k' for both the analytes showed the selectivity gained by the imprinting process. Accordingly, all interferents have small selectivity ($k' <$ 5.3%) on the proposed sensor and that too washable with water.

3.5. Stability and reproducibility

The imprinted electrochemical sensor exhibited satisfactory stability. The experimental results showed that the modified electrode was able to maintain its original behaviour without showing any deviation in current. The modified electrode was found to be rugged in aqueous sample for the period of three weeks. However, after three weeks, the current response was decreased only about 2.1% to its initial response. The reproducibility of the imprinted sensor was investigated by assaying 15.15 ng mL^{-1}, D-Ser and L-Ser each, in 0.01 M phosphate buffer solution. Accordingly, DPASV runs using five MIP sensors prepared under the same procedure were identical. In fact the recovery standard deviation (*RSD*) of 0.43% was noticed, which indicated a good sensor-to-sensor reproducibility and excellent recognition ability. Unfortunately, the earlier serine sensors reported in the literature (Table S4) did not specify their reusability and endurance, except nickel-nickel oxide half- nanotubes/boron dipped diamond electrode (Dai et al., 2015) which explored sensor-to-sensor stability with RSD less than 5.0%. In view of this, the proposed sensor could be termed to be highly stable in terms of durability and repetitiveness for D- and L-Ser measurements.

3.6. Analytical validation

The analytical performance of the proposed method was statistically

Table 1
Sample behaviour.

Sample	Analyte/s	Dilution factor	Regression equation	Linear range (ng mL^{-1})	Recovery[a] (%)	*LOD*[b] (ng mL^{-1})	Endogenous concentration[c] (ng mL^{-1})
Aqueous	D-Ser	–	ΔI (μA) = (0.502 ± 0.002) + (0.004 ± 0.034) C	0.83– 20.63	98–101	0.24	–
	L-Ser	–	ΔI (μA) = (0.490 ± 0.002) + (0.008 ± 0.029) C	0.87– 20.45	98–101	0.25	–
CSF	D-Ser	230	ΔI (μA) = (0.530 ± 0.002) + (0.005 ± 0.036) C	0.86 – 20.78	99–101	0.25	1.95×10^2
	L-Ser	2240	ΔI (μA) = (0.510 ± 0.003) + (0.004 ± 0.030) C	0.88–20.87	99–102	0.27	19.50×10^2
Blood serum	D-Ser	3	ΔI (μA) = (0.515 ± 0.003) + (0.009 ± 0.012) C	0.88– 20.55	99–101	0.26	0.02×10^2
	L-Ser	188	ΔI (μA) = (0.531 ± 0.002) + (0.006 ± 0.004) C	0.87– 20.45	99–101	0.25	1.60×10^2
Pharmaceutical	D-Ser	3110	ΔI (μA) = (0.510 ± 0.002) + (0.007 ± 0.010) C	0.85– 20.65	98–101	0.24	2.76×10^3
	L-Ser	3110	ΔI (μA) = (0.108 ± 0.002) + (0.006 ± 0.020) C	0.89– 20.50	99–102	0.28	2.76×10^3

[a] % Recovery = (amount of analyte determined / amount of analyte taken) x 100.
[b] *LOD* based on the minimum distinguishable signal for lower concentrations of analyte (S/N = 3, 95% confidence level).
[c] Original concentration obtained by multiplying lower quantitation limit with the dilution factor.

compared to a validated electrochemical nickel – nickel oxide half-nanotube-modified boron-doped diamond electrode (Dai et al., 2015), using Student's *t*-test [(t_{cal} 2.13 < t_{tab} 2.77)], at the confidence level of 95%. Although both electrodes are adjudged reproducible, the present sensor can detect both enantiomers in the wide concentration range, with quantitation limit as low as 0.87 ng mL^{-1}, requisite to diagnose schizophrenia and epilepsy. In order to validate the analytical applicability of proposed sensor, the quantitative determinations of D-Ser and L-Ser were successfully made in real samples (blood serum, CSF, and pharmaceutics) (Table 1). For demonstrating the feasibility of analysis of both the templates, we have diluted the real samples with water so as to mitigate the matrix effect and to move the analysis in the detection range. Quantitative DPASV measurements are being shown with real sample, CSF (Fig. S8 A–B), blood serum (Fig. S9 A–B), and pharmaceutics (Fig. S10 A–B). The almost equivalent slopes of the respective linear calibration equations (Table 1) indicate negligible matrix complications. Compared with many previously reported electrochemical sensors for D-Ser and L-Ser (Table S4)., the proposed sensor exhibits a wider linear range ((0.83–20.63 ng mL^{-1} for D-Ser) and 0.87–20.45 ng mL^{-1} for L-Ser) and a lower detection limit (0.24 ng mL^{-1} for D-Ser and 0.25 ng mL^{-1} for L-Ser). Insofar as the cost of fabrication of the proposed sensor is concerned, the Lbl immobilised of imprinted material on a single electrode is apparently cost-effective involving less time and labour. In addition, other techniques reported

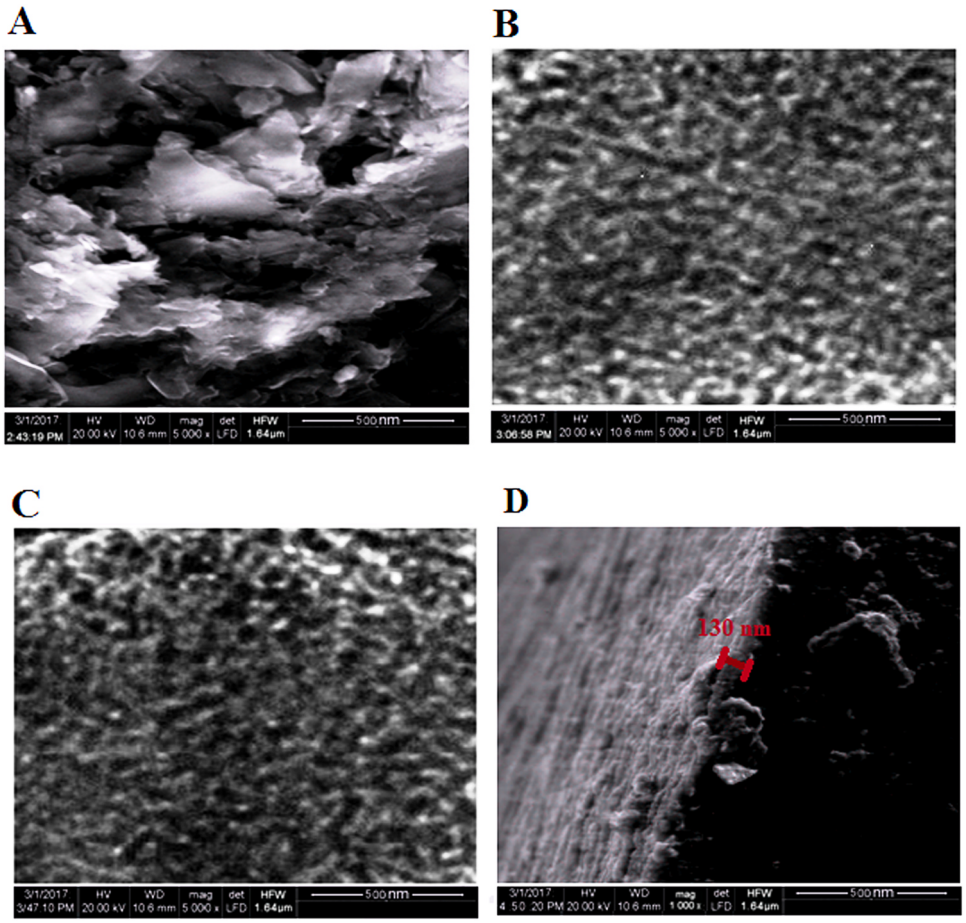

Fig. 4. SEM images: (A) acrylamide functionalised r-GO/PGE, (B) acrylamide functionalised rGO-C_{60}MIP-adduct(LbL)/PGE and (C) acrylamide functionalised rGO-C_{60} MIP(LbL)/PGE, and (D) side view of acrylamide functionalised rGO-C_{60} MIP (LbL)/PGE.

earlier were not validated with real samples (Table S4).

4. Conclusion

This work reports for the first time a novel MIP-based electrochemical sensor to quantitatively discriminate D- and L- Ser utilizing LbL approach. Since both isomers have identical redox behaviour, two distinct imprinted layers of different moieties was found to be appropriate to resolve diffusional constraint in comparison to the single layer imprinted MIP motif or double layered imprinted MIP of identical structure. In comparison to the previous work (Table S4), the proposed sensor is highly sensitive (*LOD* = 0.24 ng mL^{-1} for D-Ser and 0.25 ng mL^{-1} for L-Ser) in the wide potential range (0.83–20.63 ng mL^{-1} for D-Ser) and (0.87–20.45 ng mL^{-1} for L-Ser), with imprinting factors as high as 25.61, without limitations of regeneration, cross-reactivity, and false-positives. Thus, the high sensitivity of the measurement can be exploited for sequential analysis of D- & L-Ser using a single electrode, for the diagnosis of schizophrenia, manifested at ultra-trace level in clinical patients.

Acknowledgements

Authors thank University Grant Commission, New Delhi for granting a research fellowship to one of us (S.J). Instrumental facilities procured from Banaras Hindu University are also greatly acknowledged. We gratefully acknowledge DST-nanomission (SR/NM/NS-1212/2013 project) for financial support in the present work. We also acknowledge CSIR-SRF for providing fellowship to one of the author (S.J) and one of the co-author (K.S).

Appendix A. Supporting information

Supplementary data associated with this article can be found in the online version at doi:10.1016/j.bios.2018.09.090.

References

Antwi-Boampong, S., Peng, J.S., Carlan, J., Bel Bruno, J.J., 2014. IEEE Sens. J. 14, 5.
Bourlinos, A.B., Georgakilas, V., Mouselimis, V., Kouloumpis, A., Mouzourakis, E., Koutsioukis, A., Antoniou, M., Gournis, D., Karakassides, M.A., Deligiannakis, Y., Urbanova, V., Cepe, K., Bakandritsos, A., Zbori, R., 2017. Appl. Mater. Today 9, 71–76.
Bozdaganyan, M.E., Orekhov, P.S., Shaytan, A.K., Shaitan, K.V., 2014. PLoS One 9, 1–8.
Başkaya, Gaye, Yıldız, Yunus, Savk, Aysun, Okyay, Tugba Onal, Eriş, Sinan, Sert, Hakan, Şen, Fatih, 2017. Biosens. Bioelectron. 91, 728–733.
Bozkurt, Sait, Tosun, Berna, Sen, Betül, Akocak, S.üleyman, Mehmet, AysunSavk, Ebeoğlugil, Faruk, Sen, Fatih, 2017. Anal. Chim. Acta 989, 88–94.
Chang, K., Mei, Z., Wang, T., Kang, Q., Ouyang, S., Ye, J., 2014. ACS Nano. 8, 7078–7087.
Chernozatonskii, L.A., Kvashnin, A.G., Sorokin, P.B., 2016. Nanotechnology 27, 1–6.
Dai, W., Li, H., Li, M., Li, C., Wu, X., Yang, B., 2015. ACS Appl. Mater. Interfaces 7, 22858–22867.
Dickert, F.L., Achatz, P., Halikias, K., 2001. Fresenius' J. Anal. Chem. 371, 11–15.
Fernandes, Diana M., Nunes, Marta, Carvalho, Ricardo J., Bacsa, Revathi, Mbomekalle, Israel-Martyr, Serp, Philippe, de Oliveira, Pedro, Freire, Cristina, 2015. Inorganics 3, 178–193.
Fernandez-Gonzalez, A., Badia-Lamo, R., Diaz-Garcia, M.E., 2011. Microchim. Acta 172, 351–356.
Georgakilas, V., Bourlinos, A.B., Ntararas, E., Ibraliu, A., Gournis, D., Dimos, K., Kouloumpis, A., Zboril, R., 2016a. Carbon 110, 51–55.
Georgakilas, V., Tiwari, J.N., Kemp, K.C., Perman, J.A., Bourlinos, A.B., Kim, K.S., Zboril, R., 2016b. Chem. Rev. 116, 5464–5519.
Halim, A., Farhanah, N., Noor, A.M., Shakaff, A.Y., Deraman, N., 2013. Prod. Eng. 53, 64–70.
Halim, N.F.A., Ahmed, A.K.M.S., Islam, S., Shakaf, A.Y.M., Zakaria, Z., Derman, M.N., 2014. Adv. Mater. Res. 925, 500–504.
Hashimoto, K., Fukushima, T., Shimizu, E., Komatsu, N., Watanabe, H., Shinoda, N., Nakazato, M., Kumakiri, C., Okada, S., Hasegawa, H., Imai, K., Iyo, M., 2003. Arch. Gen. Psychiatry 60, 572–576.
Hernández, R., Riu, J., Bobacka, J., Vallés, C., Jiménez, P., Benito, A.M., Maser, W.K., Rius, F.X., 2012. J. Phys. Chem. C 116, 22570–22578.
Hummers, W.S., Offeman, R.E., 1958. J. Am. Chem. Soc. 80, 1339.
Hu, Shirong, Huang, Qitong, Lin, Yi, Wei, Chan, Zhang, Hanqiang, Zhang, Wuxiang, Guo, Zhenbo, Bao, Xiuxiu, Shi, Jiangu, Hao, Aiyou, 2014. Electrochim. Acta. 130, 805–809.
Hu, Qiong, Wang, Qiang wei, Jiang, Cuihua, Zhang, Jian, Kong, Jinming, Zhang, Xueji, 2018. Biosens. Bioelectron. 110, 52–57.
Jing, T., Wang, Y., Dai, Q., Xia, H., Niuu, J., Hao, Q., Mei, S., Zhou, Y., 2010. Biosens. Bioelectron. 25, 2218–2224.
Jegal, J.G., Lee, G.H., Son, S.H., 2007. Repub. Korean Kongkae Taeho Kongbo 2007 (1002), (KR 2007096705 A).
Koning, T.J.D., Snell, K., Duran, M., Berger, R., Poll-The, B., Surtees, R., 2003. Biochem. J. 371, 653–661.
Kouloumpis, A., Spyrou, K., Dimos, K., Georgakilas, V., Rudolf, P., Gournis, D., 2015. Front. Mater. 2, 10.
Koskun, Y., Şavk, Aysun, Şen, Betül, Şen, Fatih, 2018. Anal. Chim. Acta 1010, 37–43.
Labib, M., Sargent, E.H., Kelley, S.O., 2016. Chem. Rev. 116, 9001–9090.
Madeira, C., Lourenco, M.V., Vargas-Lopes, C., Suemoto, C.K., Brandão, C.O., Reis, T., Leite, R.E.P., Laks, J., Jacob-Filho, W., Pasqualucci, C.A., Grinberg, L.T., Ferreira, S.T., Panizzutti, R., 2015. Transl. Psychiatry 5, 1–9.
Ma, J., Guo, Q., Gao, H., Qin, X., 2013. Fuller Nanotub. Car N 23, 477–482.
Martín, A., Escarpa, A., 2014. Trends Anal. Chem. 56, 13–26.
Prasad, B.B., Jauhari, D., Tiwari, M.P., 2013. Biosens. Bioelectron. 50, 19–27.
Prasad, B.B., Jauhari, D., Tiwari, M.P., 2014. Biosens. Bioelectron. 59, 81–88.
Prasad, B.B., Jaiswal, S., Singh, K., 2017a. Sens. Actuators B: Chem. 240, 631–639.
Prasad, B.B., Singh, R., Singh, K., 2017b. Sens. Actuators B: Chem. 246, 38–45.
Roushani, M., Shamsipur, M., Pourmortazavi, S.M., 2012. J. Appl. Electrochem. 42, 1005–1011.
Saha, M., Das, S., 2014. Nanostruct. Chem. 4, 102–109.
Saraf, Nilesh, Woods, Eric, R., Peppler, Madison, Seal, Sudipta, 2018. Biosens. Bioelectron. 117, 40–46.
Singh, A.K., Singh, M., 2016. J. Electroanal. Chem. 780, 169–175.
Singh, V., Joung, D., Zhai, L., Das, S., Khondaker, Seal, S.I.S., 2011. Prog. Mater. Sci. 56, 1178.
Son, S.H., Jegal, J., 2007. J. Appl. Polym. Sci. 104, 1866–1872.
Spyrou, K., Kang, L., Diamanti, E.K., Gengler, R.Y., Gournis, D., Prato, M., Rudolf, P., 2013. Carbon 61, 313–320.
Tada, T., Ishida, Y., Saigo, K., 2006. 71, 1633–1639.
Tang, H., Radosz, M., Shen, Y., 2006. Macromol. Rapid Commun. 27, 1127–1131.
Vasapollo, G., Sole, R.D., Mergola, L., Lazzoi, M.R., Scardino, A., Scorrano, S., Mele, G., 2011. Int. J. Mol. Sci. 12, 5908–5945.
Venkatesan, G.A., Lee, J., Farimani, A.B., Heiranian, M., Collier, C.P., Aluru, N.R., Sarles, Stephen, A., 2015. Langmuir 31, 12883–12893.
Wei, Lang, Lei, Yilong, Fu, Hongbing, Yao, Jiannian, 2012. Appl. Mater. Interfaces 4, 1594–1600.
Wu, G., 2009. Amino Acids 37, 1–17.
Xu, H., Schonhoff, M., Zhang, X., 2012. Small 4, 517–523.
Xu, Z., Zhang, Y., Qian, X., Shi, J., Chen, L., Li, B., Niu, J., Liu, L., 2014. Appl. Sur. Sci. 316, 308–314.
Yáñez-Sedeño, P., Pingarrón, J.M., Riu, J., Rius, F.X., 2010. Trends Anal. Chem. 29, 939–953.
Zaidi, S.A., Shin, J.H., 2014. Int. J. Electrochem. Sci. 9, 4598–4616.

Swadha Jaiswal is currently pursuing Ph.D. at Banaras Hindu University (BHU) under the supervision of Prof. Bhim Bali Prasad. She received her B.Sc. degree in 2011 and M.Sc. degree in 2013 from BHU, Varanasi. She was the recipient of UGC Fellowship and currently getting CSIR-SRF fellowship. Her research interest lies in the field of chemical sensor development, molecularly imprinted polymers, and electro-analytical chemistry.

Richa Singh is currently pursuing Ph.D. at Banaras Hindu University (BHU) under the supervision of Prof. Bhim Bali Prasad. She received her B.Sc. degree in 2010 and M.Sc. degree in 2013 from BHU, Varanasi. She is recipient of CSIR-SRF Fellowship. Her research interest lies in the field of chemical sensor development, molecularly imprinted polymers, and electro-analytical chemistry.

Kislay Singh is currently pursuing Ph.D. at Banaras Hindu University (BHU) under the supervision of Prof. Bhim Bali Prasad. She received her B.Sc. degree in 2011 and M.Sc. degree in 2013 from BHU. She is recipient of CSIR-SRF fellowship. Her research interest lies in the field of chemical sensors, molecularly imprinted polymers, and electro-analytical chemistry.

Sana Fatma is currently pursuing Ph.D. at Banaras Hindu University (BHU) under the supervision of Prof. Bhim Bali Prasad. She received her B.Sc. degree in 2011 and M.Sc. degree in 2013 from BHU, Varanasi. She is recipient of UGC Fellowship. Her research interest lies in the field of chemical sensor development, molecularly imprinted polymers, and electro-analytical chemistry.

Bhim Bali Prasad is currently working as a professor of Analytical Chemistry in the Banaras Hindu University (BHU), Varanasi, India. He has mentored 25 Ph.D. students and published 115 research papers in several reputed international and national Journals. He received his B.Sc. degree in Chemistry in 1972 and M.Sc. degree in 1974 form BHU. He obtained his Ph.D. from BHU. He is a recipient of several national and international awards for his research contributions in Analytical Chemistry and nano-materials. His research interests include environmental chemistry, chromatography, electroanalysis, and detection principle for chemical analysis, nano-technology, and development of biomimetic nano sensors using molecularly imprinted polymers for clinical, pharmaceutical and biological analysis.